Structural Monitoring and Maintenance, *Vol. 9, No. 2 (2022) 107-127*
https://doi.org/10.12989/smm.2022.9.2.107

Damage evaluation of seismic response of structure through time-frequency analysis technique

Wen-Hui Chen[1a], Wen Hseuh[2b], Kenneth J. Loh[3c] and Chin-Hsiung Loh*[2,3]

[1]*P-Waver Inc., Taipei, Taiwan*
[2]*Department of Civil Engineering, National Taiwan University, Taipei 10617, Taiwan*
[3]*Department of Structural Engineering, University of California-San Diego, La Jolla, CA 92093, USA*

(Received May 17, 2020, Revised March 30, 2022, Accepted March 31, 2022)

Abstract. Structural health monitoring (SHM) has been related to damage identification with either operational loads or other environmental loading playing a significant complimentary role in terms of structural safety. In this study, a non-parametric method of time frequency analysis on the measurement is used to address the time-frequency representation for modal parameter estimation and system damage identification of structure. The method employs the wavelet decomposition of dynamic data by using the modified complex Morlet wavelet with variable central frequency (MCMW+VCF). Through detail discussion on the selection of model parameter in wavelet analysis, the method is applied to study the dynamic response of both steel structure and reinforced concrete frame under white noise excitation as well as earthquake excitation from shaking table test. Application of the method to building earthquake response measurement is also examined. It is shown that by using the spectrogram generated from MCMW+VCF method, with suitable selected model parameter, one can clearly identify the time-varying modal frequency of the reinforced concrete structure under earthquake excitation. Discussions on the advantages and disadvantages of the method through field experiments are also presented.

Keywords: damage detection and localization; modified continuous wavelet analysis; Novelty index; seismic response data of building; time-frequency analysis

1. Introduction

Modern monitoring systems are usually intended to ensure safety surveillance and maintenance supervision of structures, and the systems are often equipped with several instruments and sensors. But the monitoring data offer a quantity of information that is not always easy to discriminate and to understand. Every phenomenon and every parameter that can be measured is subject to "external" influence from other phenomena or other parameters which may be known or unknown and could have great influence on the data being considered. Therefore, signal processing techniques are employed on the measured data to extract the important features. To analyze the data collected from

*Corresponding author, Adjunct Professor, E-mail: lohc0220@ntu.edu.tw
[a]Principal Engineer, E-mail: wendy@pwaver.com
[b]Graduate Student, E-mail: r04521225@ntu.edu.tw
[c]Professor, E-mail: kenloh@ucsd.edu

http://www.techno-press.org/?journal=smm&subpage=7 ISSN: 2288-6605 (Print), 2288-6613 (Online)

the monitoring system, among the structural health monitoring (SHM) techniques, the vibration-based analysis tools become more and more popular because the methods can provide a fast and direct observation of the current situation of structure. Through the direct analysis on the vibration measurements, engineer can immediately detect the damage situation of the structure before it can be observed by visual inspection.

Generally, the vibration characteristics of a structure contain the global response signatures with embedded information of structural properties. Once damage occurs in the structure the dynamic response characteristics of the structure may exhibit changes in its system parameters. Changes in the structural condition will be reflected in the vibration signature, making it possible to identify the presence of damage by tracking changes to that signature. The vibration-based damage detection (VBDD) technique, through the time-frequency representation, can provide a quick and powerful tool on the analysis of time series and extract the features through time-frequency analysis. The most common method of VBDD is the estimation of the spectrogram (SP) by applying the Short-time Fourier Transform (STFT) technique (Allen *et al*. 1977) on the measurement. Besides the STFT, there were many other time-frequency analysis algorithms on vibration data, such as: Singular Spectrum Analysis (Golyandina *et al*. 2001), Continuous wavelet transform, and Wavelet packet transform (Yen *et al*. 2002), etc. Extensive research had been carried out for developing vibration-based damage detection algorithms that can relate structural dynamics changes to damage occurrence in a structure (Reda Taha *et al*. 2006).

In the past, wavelet analysis has been widely implemented for time-frequency analysis of signals, such as de-noising of signals, compression of signals and images, information retrieval from noise polluted signals, classification, and pattern recognition applications. Todorovska (2001) used the continuous wavelet transform to estimate the instantaneous frequency of signals. Lardies and Ta (2005) used a wavelet-based approach to estimate the instantaneous frequency, damping, and envelope of the system. Nair and Kiremidjian (2009) used a wavelet energy-based approach to detect the damage. Nair and Kiremidjian (2011) introduced three wavelet-based damage-sensitive features (DSFs) extracted from structural responses recorded during earthquakes to diagnose structural damage. Lee *et al* (2014) proposed a continuous relative wavelet entropy-based reference-free damage detection algorithm for truss bridge structures and showed that it was sensitive to slight damage extent for the tested damage type (i.e. loosening of bolts). Tarinejad and Damadipour (2014) used modified Morlet wavelet to estimate damping. Klepka and Uhl (2014) identified the modal parameters of non-stationary systems with the recursive method based on the wavelet adaptive filter. Guo and Kareem (2015) utilized the transformed singular value decomposition in tandem to automate the identification of analysis regions in the time-frequency domain. In the filed application, Ulriksen *et al*. (2015) applied the wavelet analysis-based damage identification method to a wind turbine blade. Since the is certainly the easiest way for building damage assessment, Application of wavelet analysis of soil-structure interaction on seismic response of base-isolated nuclear power plant was also studied by Bin Ali *et al*. (2017). Besides, a standard time-frequency analyses with amplitude normalization and reassignment method to observe smaller variations in earthquake recordings in buildings had been studied and discussed using seismic response data of Millikan library building (2010). It indicated that the physical meaning of instantaneous frequency variation is a crucial point that must be explored in depth, particularly on the seismic response of reinforced concrete structure.

Since wavelet transform (WT) is an extension of the traditional Fourier transform with the adjustable window location and window size, therefore, the method can provide a promising tool for structural health monitoring (SHM) and damage detection. To enhance the decomposition of

signal features for engineering application, a modified continuous wavelet transform (using complex Mohlet wavelet) with variable central frequency is developed in this paper. A better time-frequency representation of signal is demonstrated to replace the time-scale representation of the signal. Vitrification of the proposed method through numerical simulation is discussed. Finally, application of the proposed method to the experimental shaking table test data of a reinforced structures and the seismic response data of a building are studied for damage identification.

2. Methods on time-frequency analysis of signal

2.1 The wavelet transform

The wavelet transform is a linear transformation that decomposes an arbitrary signal *x(t)* into wavelet coefficient $W_{\psi}[x](b,a)$ and is defined as

$$W_{\psi}[x](b,a) = \int_{-\infty}^{\infty} x(t)\psi^{*}_{(b,a)}(t)dt \tag{1}$$

where $\psi_{(b,a)}(t) = \frac{1}{\sqrt{a}}\psi\left(\frac{t-b}{a}\right)$ is the mother wavelet, $\psi^{*}(t)$ is the complex conjugate of $\psi(t)$, *b* is the parameter localizing the wavelet function in time domain, and *a* is the dilatation or scale parameter defining the analysis window stretching. The selection of the proper mother wavelet is crucial for the successful implementation of a given application. In this case, the Modified Complex Morlet Wavelet (MCMW) was selected (Todorovska 2001])

$$\psi(t) = \exp(i\omega_0 t)\exp\left(-\frac{t^2}{2\sigma^2}\right) \tag{2a}$$

$$\tilde{\psi}(\omega) = \sqrt{2\pi}\sigma\, exp\left(-\frac{1}{2}(\omega-\omega_0)^2\sigma^2\right) \tag{2b}$$

where ω_0 and σ are parameters that control the central frequency and bandwidth. σ is a measure of the spread in time. The relation between scale "*a*" and frequency *f* for Morlet wavelet is given by $a = \omega_0/\omega$. In the traditional continuous wavelet transform (CWT), choosing different scale to decompose signal will result in different resolution when the frequency is change as shown in Eq. (1), besides, one needs to face how to choose proper central frequency, as shown in Fig. 1(a). Different set of (*b*, *a*) value will show different central frequency.

2.2 Modified complex morlet wavelet with variable central frequency

To improve the different resolution due to the change of frequency, from Eq. (1) by using σ=1 and three different *a*-values, both $\mathrm{Re}|\psi_{b,a}(t)|$ and $|\hat{\psi}_{(b,a)}(\omega)|$ are examined. It is observed that larger *a*-value will create a larger bandwidth in $|\hat{\psi}_{(b,a)}(\omega)|$ and as the scale parameter $a<1$ ($\omega > \omega_0$) an increase in time resolution results in a decrease in frequency resolution. In this paper, instead of choosing different scales but to choose different central frequency (f_c) to fix the scale ($a = {}^{f_0}/_{f}$

=1) when the frequency is changed, and this will change the coefficient $W_\psi[x](b,a)$ to $W_\psi[x](b,\omega)$. Fig. 1(b) shows the comparison of $\mathrm{Re}|\psi_{b,a}(t)|$ and $|\hat{\psi}_{(b,a)}(\omega)|$ considering three different central frequency (f_c) with fixed a=1.0. It is observed that the resolution in frequency domain will not change due to fix of scale for the proposed method. Of course, different σ value will change the frequency bandwidth from using MCMW.

To conduct the wavelet analysis, the loss of considerable regions of a signal is the consequence of edge effects. One possible solution to solve this problem is by padding the beginning and ending of the signal with the mirror image of the real signal (and leaving these values at both sides to be corrupted by edge effect. The length of padding data on both sides is in relating to the duration of the selected wavelet (Kijewski *et al.* 2003). The definition of time duration is defined as the time window with the amplitude $|\psi(t)|$ larger than $0.05|\psi(t)|$ (which corresponds to frequency bandwidth within $\max(|\psi(\omega)|)/\sqrt{2}$, as shown in Fig. 2(a). The relationship between the duration and σ value is shown in Fig. 2(b). Consider the Morlet wavelet with σ=2. and from Fig. 2(b) it is observed that the time duration of the Morlet wavelet is 9.8 seconds, so half of the duration (4.9 sec) of the signal will be padded to its beginning and end to compute the wavelet coefficients. Fig. 2(c) and Fig. 2(d)

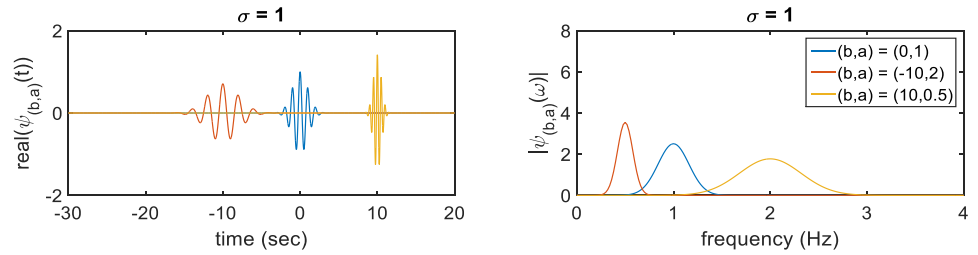

Fig. 1(a) Plot $\mathrm{Re}|\psi_{b,a}(t)|$ and $|\hat{\psi}_{(b,a)}(\omega)|$ using Mohlet wavelet using three different model parameters: (b, a)= (0,1), (-10, 2) and (10, 0.5), respectively

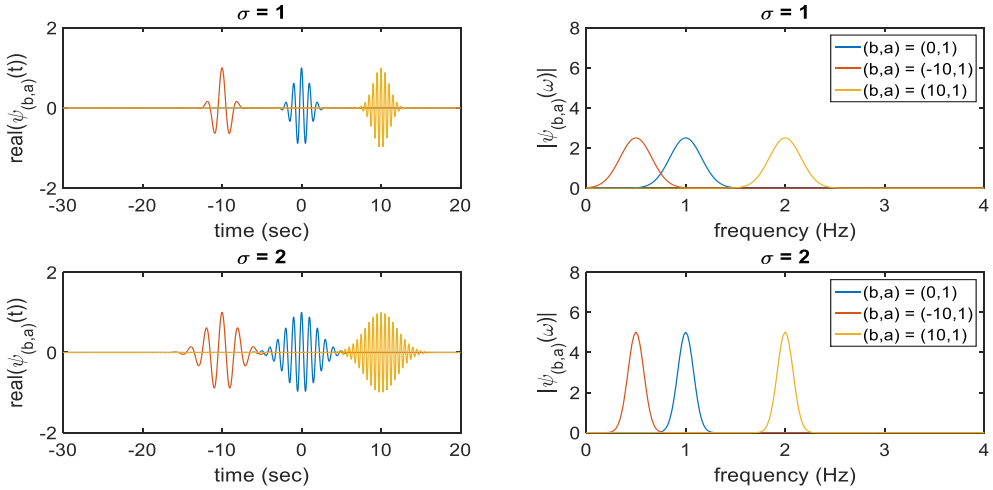

Fig. 1(b) Plot $\mathrm{Re}|\psi_{b,a}(t)|$ and $|\hat{\psi}_{(b,a)}(\omega)|$ using fixed central frequency a=1 with σ=1 (top) and σ=2 (bottom) in time and frequency domain

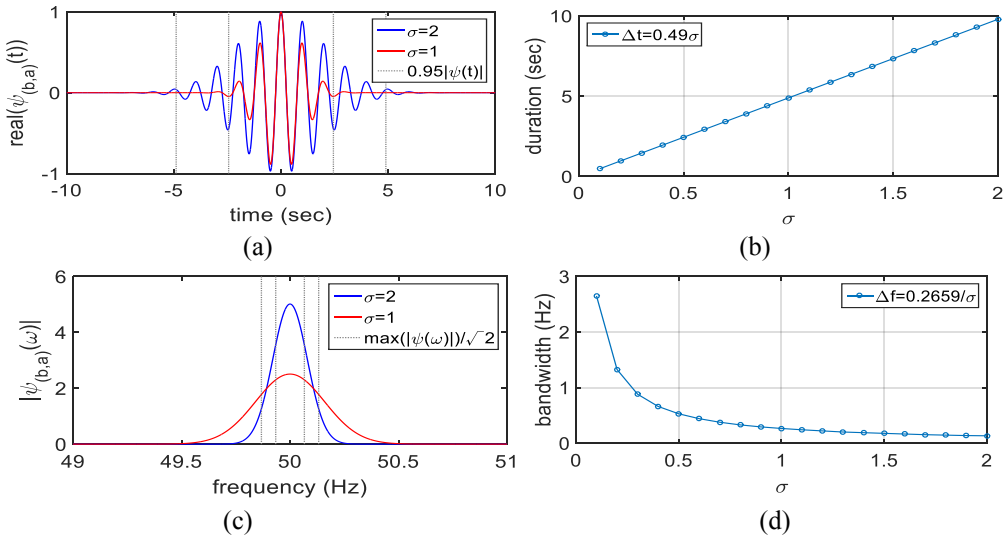

Fig. 2 (a) Plot $\mathrm{Re}\left|\psi_{b,a}(t)\right|$ for σ=2 and σ=1, (b) Plot duration versus σ for Morlet wavelet (c) Plot the amplitude of $\left|\psi_{(b,a)}(\omega)\right|$ and its frequency band for σ=1 and σ=2, (d) Plot the bandwidth vs. σ relationship

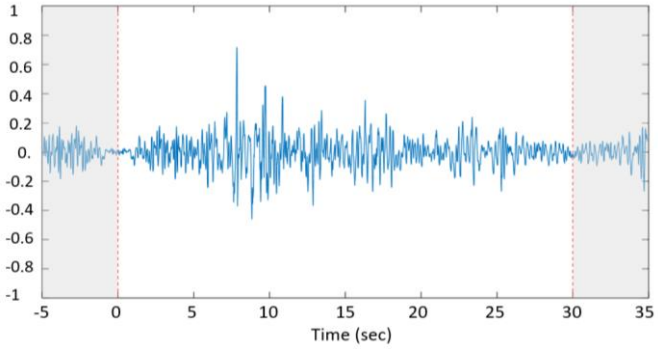

Fig. 3 Signal padding operation on both sides of the data for case of σ=2

plot the amplitude of $|\psi(b,a)(\omega)|$ and its frequency band for σ=1 and σ=2 and the bandwidth vs. σ relationship. Fig. 3 shows an example of signal padding operation for using σ=2. The padding length on both ends of the record is 4.9 sec.

To calculate the wavelet coefficient, instead of using time domain analysis directly, inverse of Fourier transform (as shown in Eq. (3)) is used.

$$W_\psi[x](b,a) = \int_{-\infty}^{\infty} x(t)\psi^*_{(b,a)}(t)dt = \frac{1}{2\pi}\int_{-\infty}^{\infty} \hat{f}(\omega)\hat{\psi}^*_{b,a}(\omega)d\omega$$
$$= \frac{1}{2\pi}\int_{-\infty}^{\infty} \hat{f}(\omega)\hat{\psi}^*(a\omega)\, e^{i\omega b}\, d\omega = FT^{-1}\{\hat{f}(\omega)\hat{\psi}^*(a\omega)\} \quad (13)$$

Where $\hat{f}(\omega)$ is the Fourier transform of the measurement and $\hat{\psi}^*(a\omega)$ is the Fourier transform of $\psi^*_{(b,a)}(t)$.

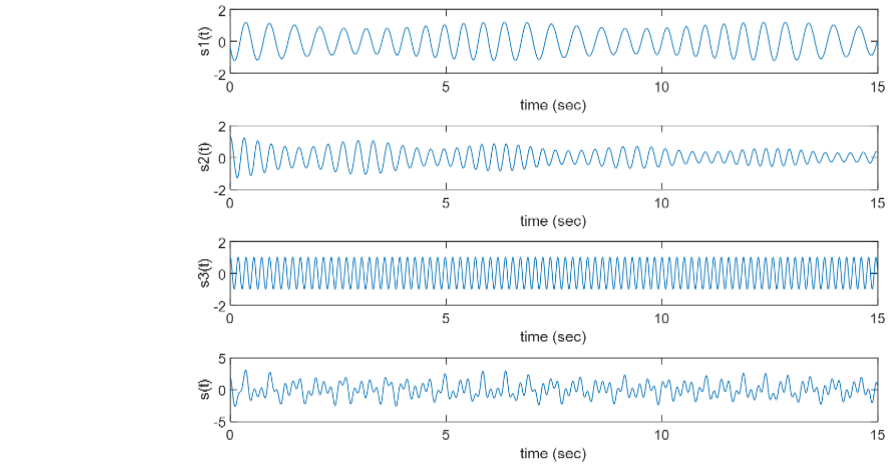

(a)

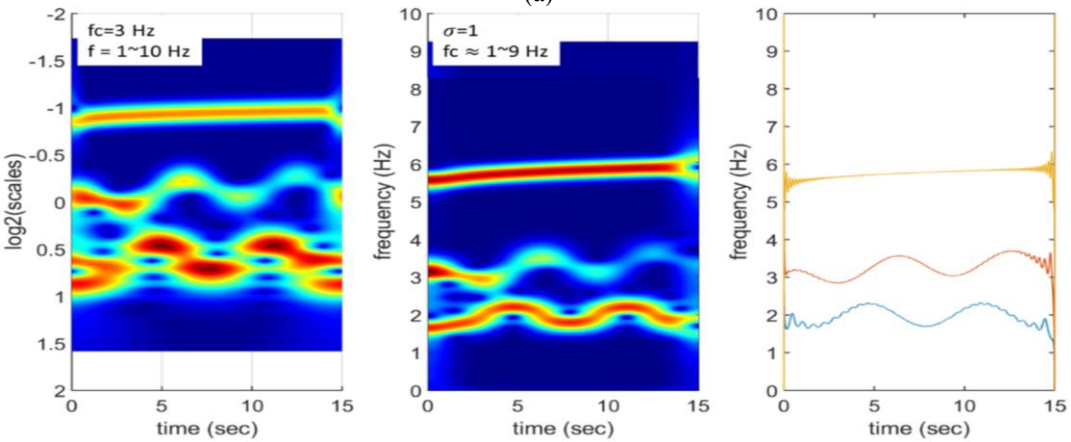

(b)

Fig. 4 (a) Synthetic time history, (b) Result of time-Frequency analysis using MCMW+VCF

3. Experimental study on time-frequency analysis of signal

To demonstrate the ability of time-frequency analysis using the proposed modified complex Morlet wavelet with variable central frequencies (MCMW+VCF), three different examples are used.

3.1 Comparison on time-frequency representation using CWT and MCMW-VCF method

To verify the successful implementation of modified complex Morlet wavelet with variable central frequencies (MCMW+VCF) for time-frequency representation, comparison between the proposed method with traditional continuous wavelet analysis (CWT) is made by using the following nonlinear signal

$$s(t) = s_1(t) + s_2(t) + s_3(t) \tag{4}$$

where

$$s_1(t) = (1+0.2\cos(2t))\cos(2\pi(2t+0.3\cos(t)))$$
$$s_2(t) = (1+0.3\cos(2t))e^{-t/15}\cos(2\pi(2.4t+0.5t^{1.2}+0.3\sin(t)))$$
$$s_3(t) = \cos(2\pi(5.3t+0.2t^{1.3}))$$

Fig. 4(a) shows the generated nonlinear signal. Application of the traditional CWT and the proposed MCMW+VCF to this nonlinear time function and calculate the time-frequency representation is shown in Fig. 4(b). The modulus of wavelet coefficients from these two methods shows that the result from CWT both time and frequency resolution is poor. Besides, the "scale" is used instead of using "frequency" in the axis of frequency presentation which make it difficult immediately convert to frequency. To which time-frequency representation through MVMW+VCF has a better presentation of the time-varying characteristics of the signal, the instantaneous frequency (IF) using Hilbert transform of each synthetic signal is also calculated for comparison. It is observed that by using general CWT, the time resolutions are poor in lower frequencies and it is difficult to identify the IF of each signal. On the contrary, by using variable central frequencies (with σ=1), one can fix the resolution and provide better time-frequency representation on the identification of IF of each signal. It is observed that using MCMW+VCF one can select a specific wavelet function with constant bandwidth along the frequency axis which can directly provide frequency scale and will have a better identification of the signal characteristics.

3.2 Time-frequency representation on the analysis of simulated nonlinear signal using MCMW-VCF

To verify the advantages of using the proposed method, a signal is designed as the combination of five individual signal (as Example 1)

$$s(t) = s_1(t) + s_2(t) + s_3(t) + s_4(t) + s_5(t) \tag{4}$$

Where

$$s_1(t) = cos(2\pi \cdot 1.5t) \qquad t \le \frac{5\pi}{2}$$
$$s_2(t) = cos(\frac{8\pi}{3}[(t-10)^2 - (2\pi-10)^2] + 6\pi(t-2\pi)) \qquad 2\pi \le t \le 4\pi$$
$$s_3(t) = cos(6 \cdot 2\pi(t + 0.1\, sin(1.5\, t))) \qquad t \le 2\pi$$
$$s_4(t) = sin(2\pi \cdot 3t) \qquad 0 \le t \le 4\pi$$
$$s_5(t) = sin(2\pi \cdot 4t) \qquad 0 \le t \le 4\pi$$

The sampling rate of this simulated signal is 100 Hz and with duration of 4π sec. The waveforms and the Fourier amplitude spectrum of $s(t)$ are shown in Fig. 5. From the observation of Fourier amplitude spectrum of the signal, one can clearly identify three major dominant frequencies with very narrow frequency band in Fourier amplitude spectrum which can be characterized as the sinusoidal signals. Besides, there are some frequency contents higher than 5.0 Hz that cannot be clearly identified (i.e., the time-varying signal). To have a better identification of the signal, first, the modified complex Morlet wavelet with variable central frequency (MCMW-VCF) on time frequency analysis was also applied. Fig. 6 shows the time-frequency representation of the signal by using three different parameters in the complex Morlet wavelet, i.e., σ=0.5, σ=1.0, and σ=2.0. It is observed that by using smaller σ-value (i.e., σ=0.5) one can have a shorter time-window of wavelet function and with poor resolution for frequency domain signal because the wavelet function will have a wider bandwidth in frequency domain. Therefore, with smaller σ-value the better

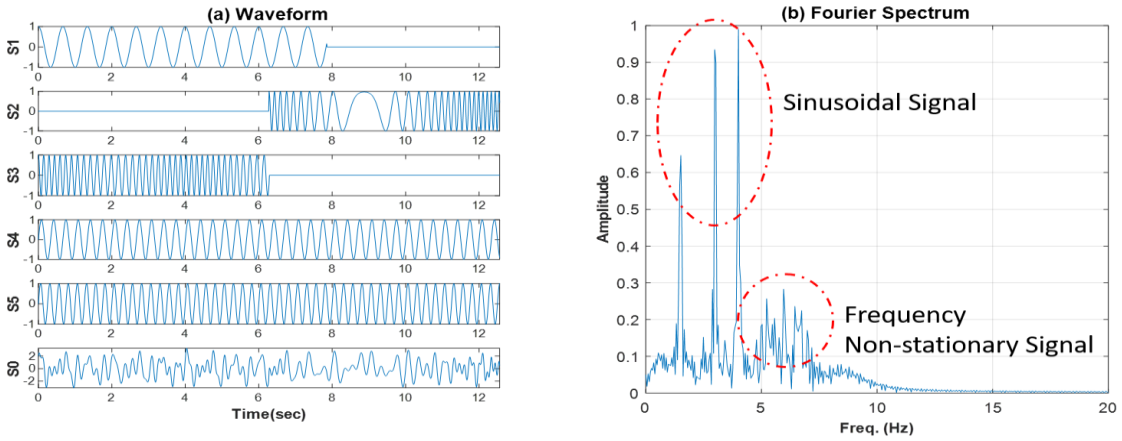

Fig. 5 Waveform and its corresponding Fourier amplitude spectrum

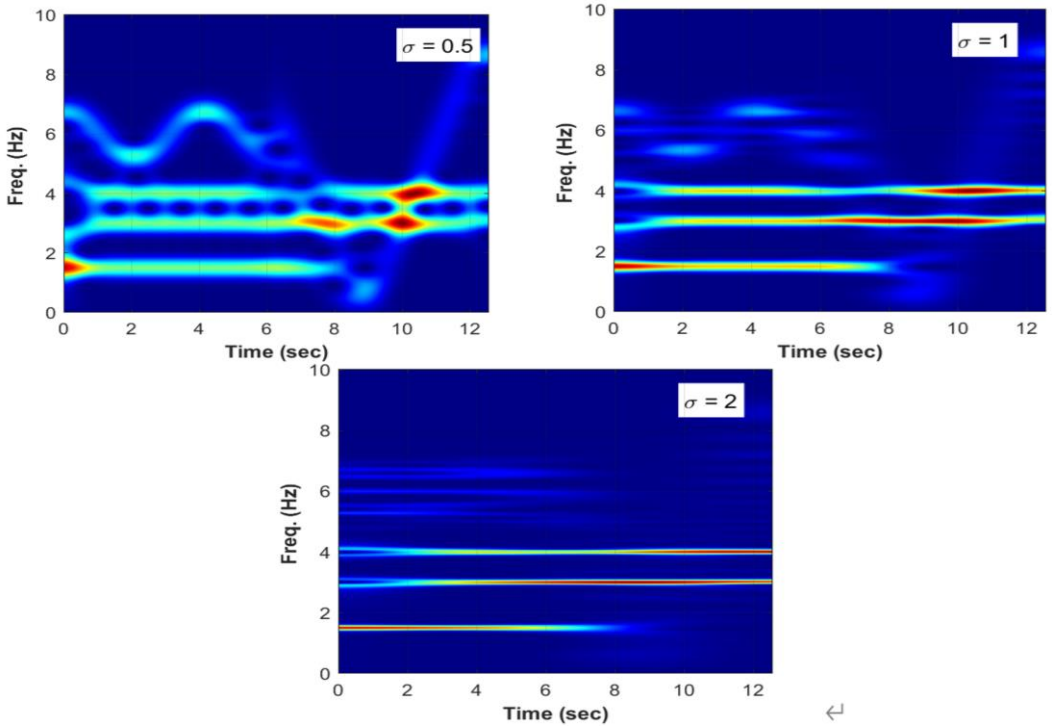

Fig. 6 Time-frequency representation using MCMW-VCF with three different σ values

precision for the identification of high frequency time-varying signal (i.e., $s_3(t)$) and the non-stationary signal (i.e., $s_2(t)$) but poor identification of close-space sinusoidal signals (due to interference). On the contrary, using larger σ-value, the time window of wavelet function is longer, therefore, a better identification for time-invariant sinusoidal signal but poor identification on high frequency time-varying signal $s_2(t)$. Since σ-value is a user-defined parameter in the MCMW-VCF time frequency analysis, it must be defined as a prior in TF analysis. Larger σ-value will have

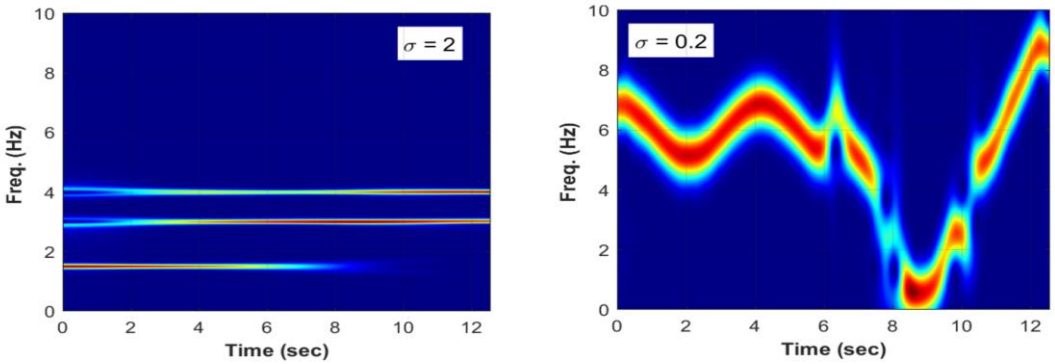

Fig. 7 (a) Spectrogram of the principal components of signal (extracted from SSA), (b) Spectrogram of the residual signal using MCMW-VCF with σ=0.2

a longer wavelet function in time domain and narrower in frequency domain, and smaller σ-value will have a shorter wavelet function in time domain and longer frequency band in frequency domain.

From Fig. 6 one can easily identify the sinusoidal signal, $s_1(t), s_4(t)$ and $s_5(t)$ by using σ=2, while the non-stationary signals $s_2(t)$ and $s_3(t)$ cannot be detect clearly. Even with smaller σ value the time-frequency representation is not so clear to detect the non-stationary signal too. An extension of MCMW-VCF method is employed. Since singular spectrum analysis (SSA) technique can decompose the original series into the sum of a small number of independent and interpretable components such as a slowly varying trend, oscillatory components and a structureless noise through the singular value decomposition (SVD) of the constructed data Hankel matrix, therefore, the SSA can be employed in advance to extract the sinusoidal signals from the original data. Fig. 7(a) shows the spectrogram of the extracted signals $s_1(t), s_4(t)$ and $s_5(t)$. Then the MCMW-VCF can be used to the residual signal and presents the time-frequency representation of the residual signal, as shown in Fig. 7(b). Considering the time-varying characteristics of the residual signal, a smaller σ value is used to generate the time-frequency figure. The time-frequency representation of residual signals can clearly identify the non-stationary signals by using smaller σ-value in MCMW-VCF.

3.3 Analysis of seismic response data from shaking table test of a RC frame

Different from the simulated data, a shaking table test data from a one-story two-bay RC frame (Fig. 8(a)) with an overall height of 2 m, and an approximate weight of the frame was 6454 kg is used. The RC specimen was mounted on a shaking table for testing. For the shake table test, 12 accelerometers were used to measure the acceleration. Four lateral LVDTs (Linear Variable Differential Transformers) were instrumented to acquire displacement response. The input ground motion was selected from 1999 Taiwan Chi-Chi earthquake (Station: TCU082). The frame (defined as RCF) was tested using input excitation from the base with PGA=1287 gal. The sampling frequency for the recorded devices is 200 Hz. The maximum inter-story drift ratio for this RCF test case is 4.46%. The restoring force diagram of the test specimen (plot the absolute acceleration response from the top of the frame structure as well as the relative displacement response) is shown in Fig. 8(b). From the restoring force diagram, it is observed that a significant permanent deformation as well as a severe inelastic response of the structure during earthquake excitation can be observed after the test. The proposed wavelet analysis will be used to generate the time-frequency

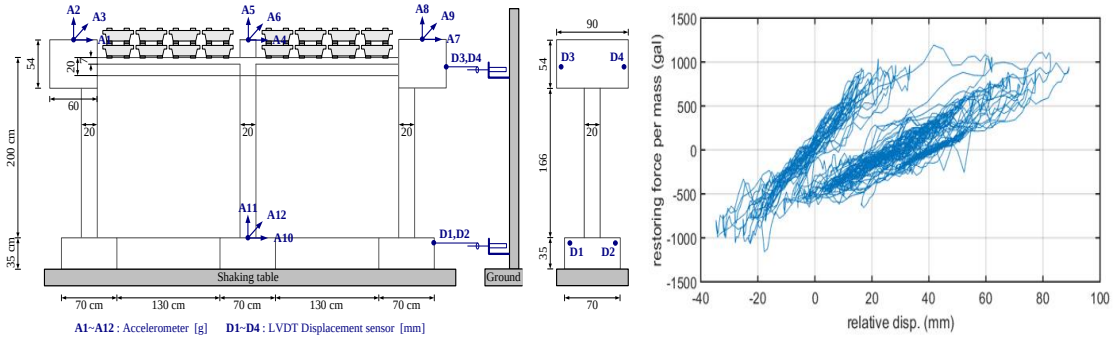

(a) (b)

Fig. 8 (a) Schematic diagram of RC frame, (b) Restoring force diagram of RC frame under earthquake excitation with PGA=1287 gal

distribution of the response data for damage identification.

Based on the recorded vibration data, the identified time-varying system natural frequency of the RCF structure subjected to ground excitation level of 1287 gal of earthquake can be viewed from the ridge of the time-frequency representation. Fig. 9(a) shows the measured acceleration response of the test frame. The proposed MCMW+VCF method is employed directly to the acceleration response data of the test frame. Fig. 9(b) is the traditional analysis using CWT and Fig. 9(c) and Fig. 9(d) show the developed time-frequency representation using MCMW+VCF method with σ=1.0 and σ=2.0, respectively. It is observed that the results from the time-frequency representation using MCMW+VCF method, depends on the selected model parameter σ in the complex Morlet wavelet, will show different resolution in the visualization of time-frequency distribution. Using larger σ value will create a longer the time duration which will provide smoother modulus in wavelet spectrum along time-axis and will have a higher resolution along the frequency representation. On the contrary, smaller σ value will have a higher resolution in time domain but provide a poor resolution in frequency domain. If there is a purse occurred in the time domain (such as a sudden crack appear in the concrete structure due to excitation), to explore this pulse from time domain, it is necessary to select a smaller σ value for analysis. Therefore, this time-frequency representation can provide the data to have a quick estimation on the system instantaneous frequency through the edge of the modulus in time-frequency representation. For this test case on reinforced concrete frame, it is observed that the system natural frequency began to decrease starting at time $t \approx 30.\ sec$ while the significant acceleration response start appears. This example also shows that by using the MCMW-VCF method on time-frequency analysis of data, with suitable selection of σ-value in wavelet function, one can immediately identify the system time-varying frequency and provide a quick damage identification of the structure. To enhance the time-varying system frequency the concept to develop the instantaneous frequency will be introduced in the following section by using the time-frequency distribution.

4. Structural health monitoring using time-frequency representation

Through experimental verification on using the MCMW+VCF wavelet transform, one can detect the time-varying signal characteristics as well as time-frequency representation of signals. Based on

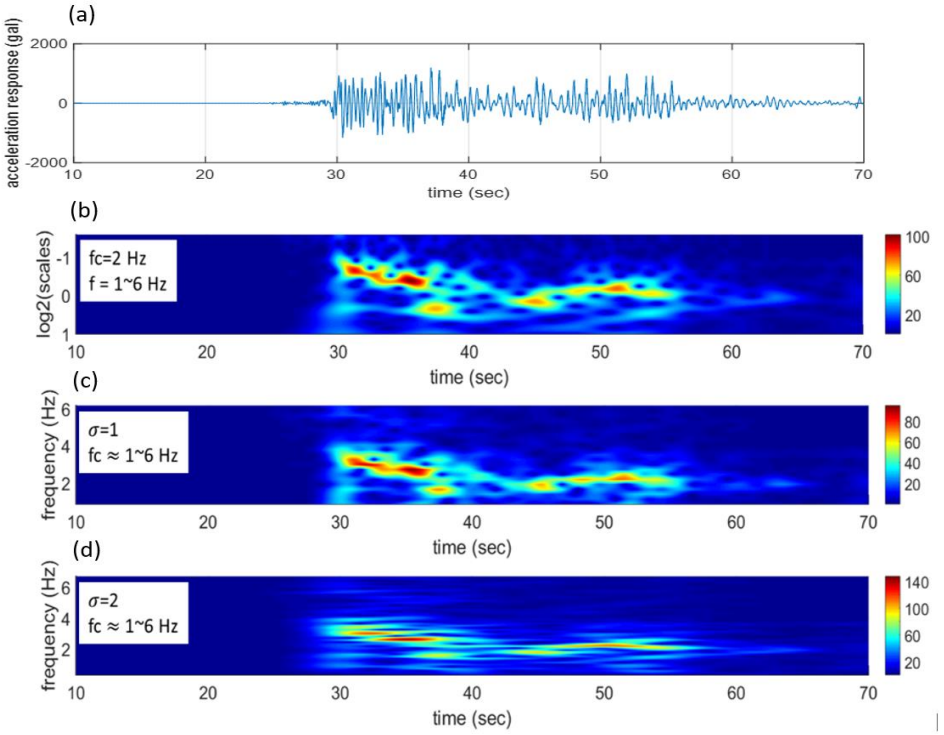

Fig. 9 (a) Acceleration response of the test specimen, (b) Scalogram developed using CWT, (c) Spectrogram using MCMW-VCF with σ=1.0, (d) Spectrogram using MCMW-VCF with σ=2.0

the time-frequency analysis from the collected data of structural response, two different indices are proposed for the damage assessment of the structure.

4.1 Estimation the instantaneous frequency

The instantaneous frequency can provide the information of structural model frequencies vary with time, a tendency to identify the system nonlinearity, a rough assessment of damage severity, and also a clearer representation for spectrogram because it is unapparent in comparatively small amplitude data. From the analysis data using MCMW+VCF the most straight forward method to extract the instantaneous frequency is from the ridge of the time-frequency representation of a signal. Basically, the ridge is the frequency f where maximum amplitude of the modulus of wavelet coefficients for each time t. This method is based on spectrogram generated from MCMW-VCF method from which the energy of the signal which concentrate near its instantaneous frequency in a narrow time interval can be identified. To reduce the noise effect and the fluctuant of the identified instantaneous frequency, a smoothed method using a time-varying mean procedure to eliminate the fluctuations, which is called the pseudo-instantaneous frequency (pseudo-IF), is used and defined as

$$\hat{f}(t) = \frac{\int_{-f_L}^{f_U} f\, H_A(t,f)\, df}{\int_{-f_L}^{f_U} H_A(t,f)\, df} \tag{5}$$

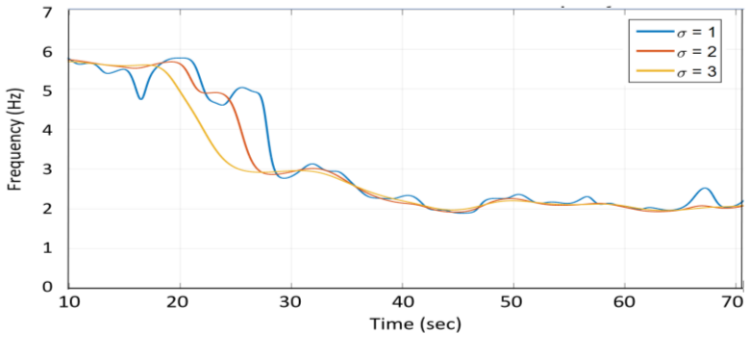

Fig. 10 Identified instantaneous frequency using MCMW+VCF time-frequency analysis

where $H_A(t,f)$ is the modulus of wavelet coefficients defined as

$$H_A(t,f)=\left|W_\psi[x](t,f)\right| \tag{6}$$

In Eq. (5), starting from the frequency at ridge of the spectrogram at t=0.0 and f_L and f_U are the lower bound and upper bound of frequency range, respectively. In here, the frequency bandwidth of $\pm 5\Delta f$ is selected. To estimate the instantaneous frequency, the centroid (or defined as the instantaneous frequency at each specific time) of the time-frequency representation at each instant of time is determined and identified as instantaneous frequency. In some cases, the decrease of system frequency may drop outside the pre-defined frequency band, therefore, the frequency band may be expended to from $10\Delta f$ to $20\Delta f$ (for a single structural modal frequency), where Δf is the bandwidth of the selected wavelet function.

Fig. 10 shows the identified instantaneous frequency of the RC frame (Fig. 8(a)) during earthquake excitation by using the result form MCMD+VCF time-frequency representation (from Figs. 9(b) and 9(c)). Different wavelet model parameter is used from the time-frequency distribution (with σ=1, 2 and 3 respectively). Larger σ value the smoother of the time frequency distribution along time axis will be. Significant of degradation of modal frequency between time t=20 sec and 30 sec are observed.

4.2 Calculate Novelty index (reference-based index) for structural damage assessment

Besides the damage assessment of structural through the identification of degradation of system dominant frequency from the seismic response data of structure, the spectrogram developed from the wavelet coefficients of the response of white noise excitation can also be used for damage localization, or alternatively, through Novelty index to detect damage location. Novelty detection aims to establish simply whether a new data pattern is significantly different from a previous data pattern. Consider the white noise response measurement before and after an earthquake excitation, based on the time-frequency distribution using MCMW+VCF method, the Novelty index (*NIn*) is defined as

$$NIn_i=\frac{\sum_t\sum_j\left|H_A^i(t,f_j)-H_A^{ref}(t,f_j)\right|}{\sum_t\sum_j\left|H_A^{ref}(t,f_j)\right|},\ i\text{: for test case } i \tag{7}$$

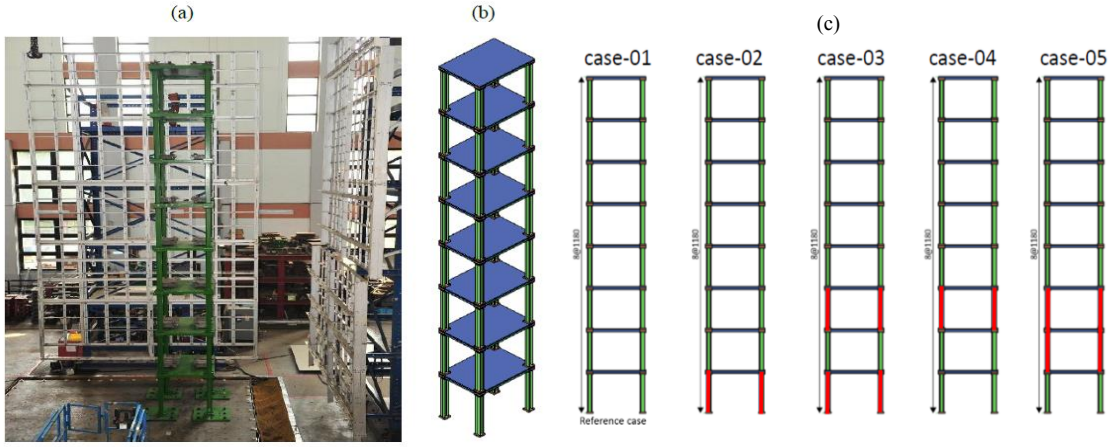

Fig. 11 (a) Photo of the 8-story test structure, (b) Dimension of the test structure, (c) different damage scenario with the change of column size (indicated by different color)

where $H_A(t,f) = \left|W_\psi[x](t,f)\right|$ is the modulus of wavelet coefficients, $H_A^{ref}(t,f)$ is refer to as the undamaged reference data, and f_j is the selected frequency band from the marginal spectrum. Novelty index can compare not only the frequency shift but also the energy changes due to the damage.

To verify the proposed NI for damage localization, shaking table test on an eight-story scaled-down structure consisted of a single bay with a 1.1 m×1.5 m floor area and a story height of 1.18 m was conducted, as shown in Fig. 11. The lumped mass of each floor was 500 kg. Low-level white noise excitations from shaking table tests were applied to the structure. A total of 16 accelerometers were installed in the structure, with two accelerometers placed on each floor along the direction of base excitation to collect the acceleration response. A duration of 120 seconds of white noise base motion was applied with a peak ground acceleration (PGA) of 50 gal only in the direction of the weak *x*-axis. The lateral acceleration of the building was measured from each floor with a sampling rate of 200 Hz. Table 1a shows the test protocol. It is observed that the structural system was modified by changing the column stiffness in different floor during a sequence of base excitation (both under earthquake and white noise base excitation). In this study, a total of five tests from white noise excitation were selected for analysis, as shown in Table 1(b). In between these five tests, several more earthquake excitations were applied to the structure. In these five test cases, reducing the column size on different floors simulated a different damage scenario, as shown in Table 1(b) (from size C1 to size C2). The identified system dominant frequencies using white noise

To verify the proposed NI for damage localization, shaking table test on an eight-story scaled-down structure consisted of a single bay with a 1.1 m×1.5 m floor area and a story height of 1.18 m was conducted, as shown in Fig. 12. The lumped mass of each floor was 500 kg. Low-level white noise excitations from shaking table tests were applied to the structure. A total of 16 accelerometers were installed in the structure, with two accelerometers placed on each floor along the direction of base excitation to collect the acceleration response. A duration of 120 seconds of white noise base motion was applied with a peak ground acceleration (PGA) of 50 gal only in the direction of the weak *x*-axis. The lateral acceleration of the building was measured from each floor with a sampling rate of 200 Hz. Table 1a shows the test protocol. It is observed that the structural system was

Table 1 (a) Test protocol of the 8-story steel structure, (b) Five different test cases (with change of column member stiffness, (c) identified modal frequencies of the test structures

(a)

Case Number	Type of Excitation	PGA (gal)
Case01	**White noise (WN4)**	50
Case02	Kobe EQ	100
	EI Centro EQ	100
	TCU076 Chi-Chi EQ	100
	White noise (WN2)	50
Case03	Kobe EQ	50
	EI Centro EQ	50
	TCU076 Chi-Chi EQ	50
	White noise (WN2)	50
Case04	EI Centro EQ	50
	TCU076 Chi-Chi EQ	50
	Kobe EQ	50
	White noise (WN2)	50
Case05	EI Centro EQ	50
	TCU076 Chi-Chi EQ	50
	Kobe EQ	50
	White noise (WN2)	50

(b)

Case No.	1F	2F	3F	4F	5F	6F	7F	8F
Case01	C1	C1	C1	C1	C1	C1	C1	C1
Case02	C2	C1	C1	C1	C1	C1	C1	C1
Case03	C2	C1	C2	C1	C1	C1	C1	C1
Case04	C1	C1	C2	C1	C1	C1	C1	C1
Case05	C1	C2	C2	C1	C1	C1	C1	C1

Note: M1 – Additional 500 kg Mass Block was added on each floor
C1 – H-type Column (Strong-axis); C2 – Rectangular Column

(c)

Freq.(Hz)	Case1 (WN04)	Case2 (WN02)	Case3 (WN02)	Case4 (WN02)	Case5 (WN02)
Mode 1	1.853	1.5226	1.3448	1.611	1.3857
Mode 2	6.7743	4.9325	4.8444	6.2529	5.4697
Mode 3	13.0226	10.8636	7.4909	11.2742	8.789
Mode 4	19.1637	16.3746	14.761	14.8921	14.8747
Mode 5	25.734	23.3363	22.089	23.8693	19.5108
Mode 6	31.9838	30.8392	25.6385	30.1364	23.7365

modified by changing not only the column stiffness during a sequence of base excitation (earthquake and white noise). In this study, a total of five tests from white noise excitation were selected for analysis, as shown in Table 1(b). In between these five tests, more several earthquake excitations were applied to the structure. In these five test cases, test data from each test with different reduced column size are listed in Table 1(c). The change of modal frequencies is obvious among different test case which can indicated the damage situation.

Based on the white noise response data among each test, the Novelty Index is used for damage localization. Time-frequency distribution for each test is generated using the proposed two methods. Consider the test case1 as the reference, Fig. 12 show the Novelty Index of different floor from different test case using MCMW+VCF generated time-frequency distributions. As shown in Fig. 12, large Novelty Index at a sensing node indicated where the location of damage appeared. For example, in test case 4 the change of member stiffness was at 3rd floor, while using the NI from one can clearly identify the large NI at 3rd floor. The result shows a close consistent with the damage scenario as indicated in Table 1b. This shows that by using the pattern recognition technique (NI) from each sensing node and compare with the reference node, one can identify the damage location easily.

5. Application to building seismic response data

To verify the applicability of the proposed method using MCMW+VCF, seismic response data of three building are used in this study: the first one is the 7-story hotel building, the second one is the 6-story school building and the third one is a 4-story school building subject to a series of seismic events. Based on the seismic response data collected from the floor acceleration, damage

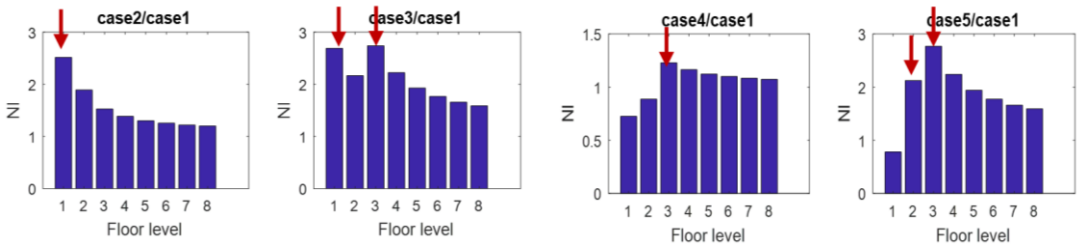

Fig. 12 Plot the novelty index for damage localization of the 8-story steel frame among 4 different damage test cases (Case01 is used as a reference case) using time-frequency distribution developed from MCMW+VCF. (Note: Arrow indicates the damage location: change of column stiffness)

Table 2 List of earthquake event from Van Nuys building for analysis

Date	Earthquake	Epic. (Fault) Dist. (km)	Peak Acceleration (g)		Date
			Ground	Struct.	Raw data
1994/6/17	Northridge #	7.0 (1.7)	0.47	0.59	V(broken)
2014/3/17	Encino #	9.8 (-)	0.144	0.219	v (Missing CH:8, 13)

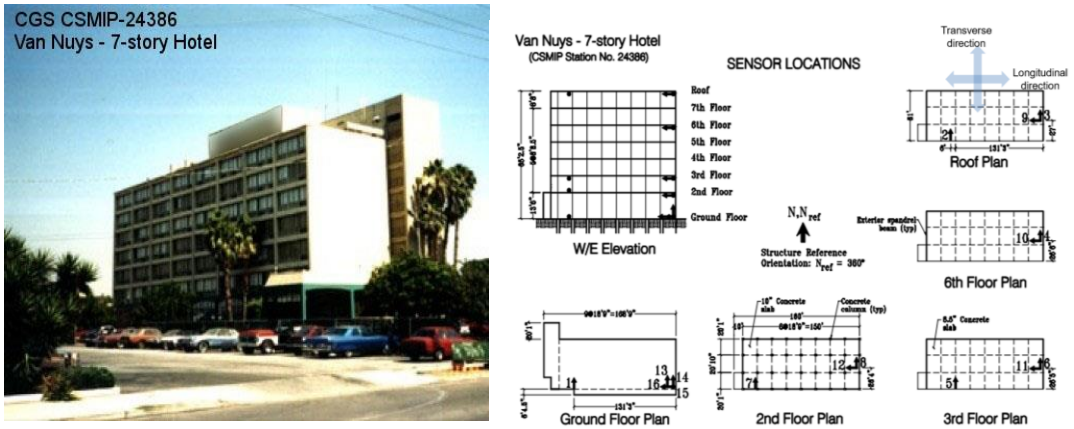

Fig. 13 Layout of strong motion instrumentation in the 7-story Van Nuys building

identification using time-frequency analysis will be discussed.

5.1 Analysis the 7-Story Van Nuys Building

The Van Nuys building in Los Angeles area was instrumented with 16 accelerometers in 1980 by CSMIP. Fig. 13 shows the instrument layout in the building with 16 accelerometers distributed across five levels. The building was repaired and strengthened with concrete shear walls after the 1994 Northridge earthquake. Among all the seismic event recorded from the building, two seismic events (as shown in Table 2) were selected for the analysis in this study. Based on the recorded seismic response data, the time-frequency analysis on the recorded roof acceleration response of the building was generated. The MCMW-VCF method was used to generate the time-frequency representation. Fig. 14(a) shows the spectrograms calculated using the recorded data from Channels

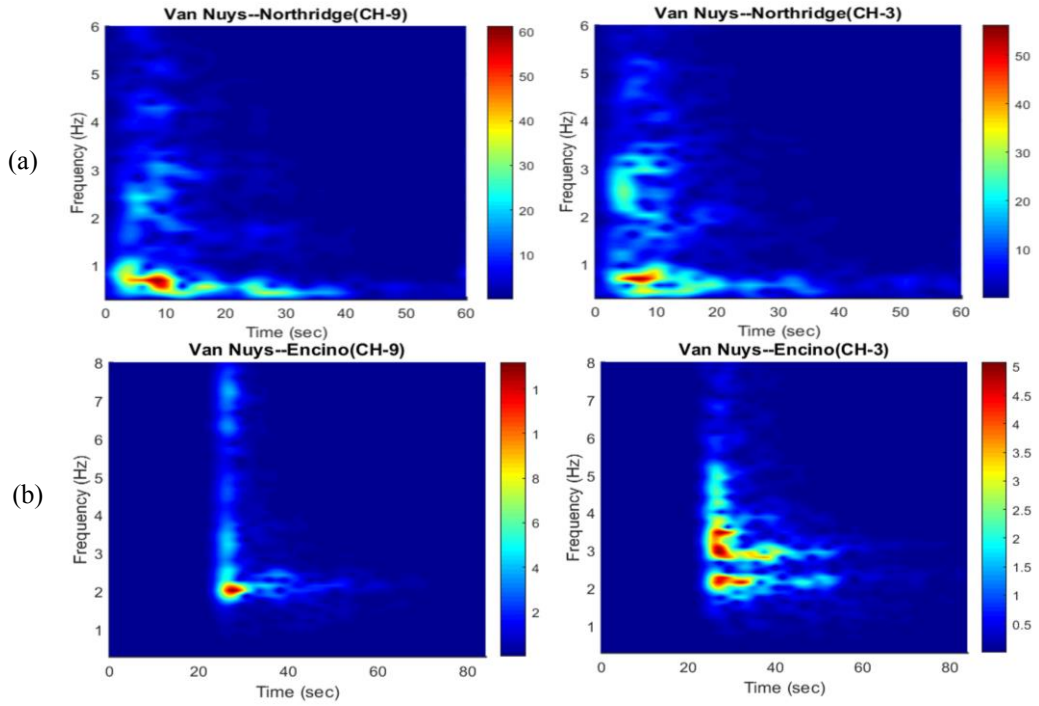

Fig. 14 Spectrograms of Channels 3 and 9 of the Van Nuys building corresponding to two seismic events: (a) Northridge earthquake and (b) Encino earthquake

9 and Channel 3 of the Northridge earthquake, while Fig. 14(b) shows the spectrograms for the Encino earthquake data; all these channels corresponded to the roof response data. A comparison between these two sets of event data (spectrogram) shows that a significant change in the fundamental dominant frequency (or from the ridge of the spectrogram) from about 0.5 Hz to 2.0 Hz. This result is expected and is consistent with the retrofit performed after the Nothridge earthquake, which would increase the stiffness of the structure and hence its dominant frequency. It indicated that by using the proposed time-frequency analysis of response data, one can easily identify the time-varying characteristics of the building through visualization.

5.2 Analysis the seismic response data of a 6-story RC building

Seismic data collected from a 6-story RC building in the campus of National Chung Hsing University (Taiwan) before (Event-9 weak motion 1996/3/5) and during the Chi-Chi earthquake (Event-13 1999/9/20 Chi-Chi earthquake) will be studied using wavelet analysis. The location of the sensing units is distributed on the basement, 1st floor, 4th floor and 7th floor, as shown in Fig. 15(a). Roof (sensor #21) and basement (sensor #26) acceleration response data collected from these two events is also shown in Fig. 15(b). Due to the complicated geometry of the structural system, the average of roof acceleration response along X-direction (i.e., average of sensor #22 and #19) and along Y-direction (i.e., average of sensor #21 and #18) are used. Fig. 16 shows the time-frequency representation of the roof response in both X- and Y-direction for these two selected seismic events. From the result of small earthquake event the identified instantaneous frequency in

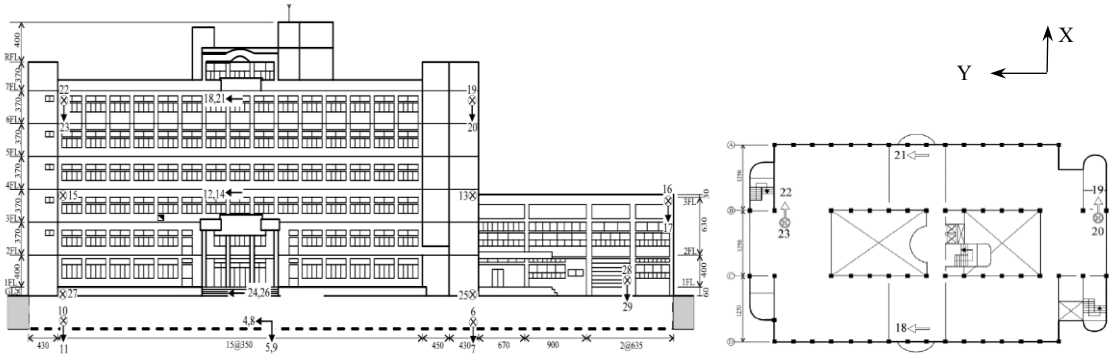

Fig. 15(a) Distribution of accelerometer in the 6-story building and the sensor distribution on the roof

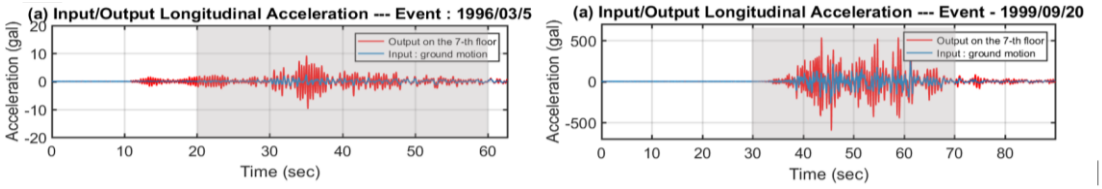

Fig. 15(b) Roof (sensor #21) and basement (sensor #26) acceleration response data collected from two seismic events. The gray-marked duration indicated the duration data for analysis

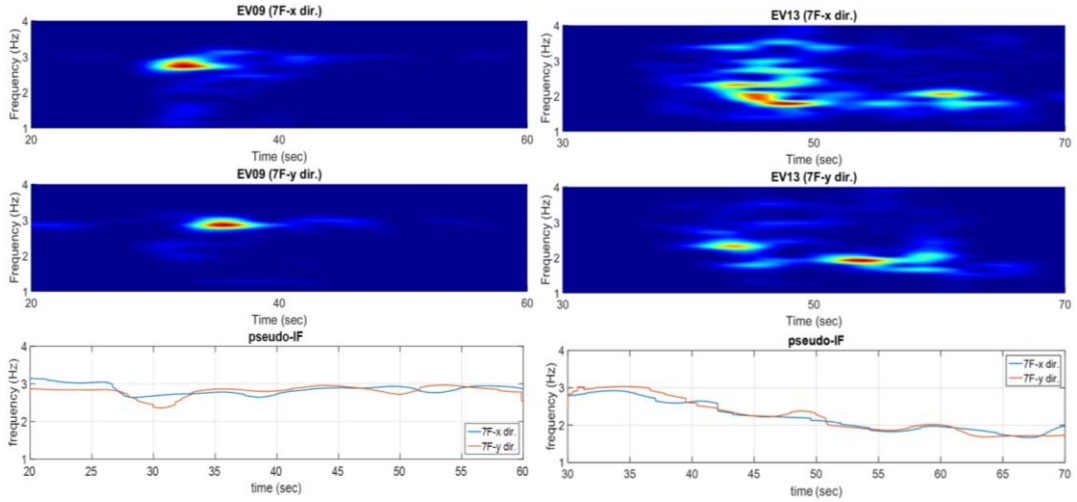

Fig. 16 Plot the time-frequency distribution from the roof response of two seismic event data (EV09:1996-03-05 and EV13:1999-09/20 earthquakes) along X-direction and Y-direction. The extracted instantaneous frequency of the signal is also shown

both directions is quite stable during the excitation (left-hand side of Fig. 16). Under strong motion, the degradation of the building dominant frequency is observed (right-hand side of Fig. 16). This is mainly dominated by the permanent and transient variations of the structural stiffness (can also be observed from the identified time-varying system natural frequency using recursive subspace identification (Chen *et al*. 2018)). In case of strong shaking like those produced by the Chi-Chi

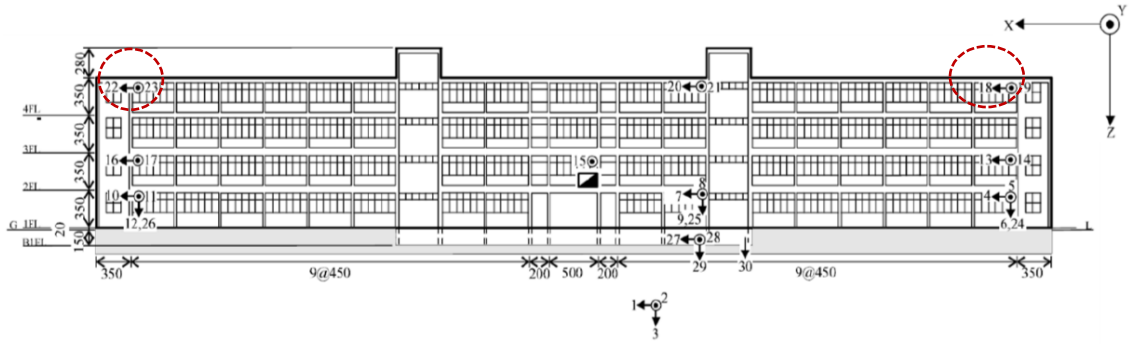

Fig. 17(a) distribution of accelerometers in the 4-story elementry school building

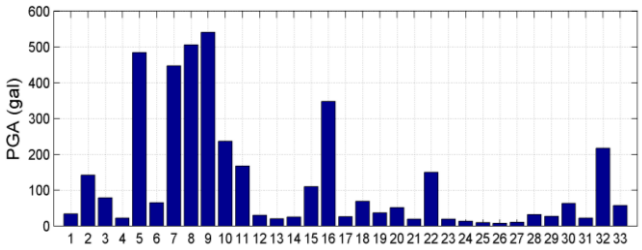

	Date	Magnitude	Depth
*Event-4	1996-09-05	M=7.07	H=14.75 km
* Event-5	1999-09-21	M=7.3	H=8.0 km
*Event-6	1999-09-21	M=6.59	H=8.57 km
*Event-13	2006-12-20	M=6.99	H=50.22 km
*Event-31	2010-10-02	M=5.09	H=19.38 km

Fig. 17(b) (a) Distribution of accelerometer in the Ming-Li elementary school building.(b) Distribution of peak acceleration & collected earthquake events from the building

earthquake, the time-frequency representation is useful to obtain a relevant interpretation of the resonance frequency variations during earthquakes. Through the comparison between the time-frequency distribution of weak motion and strong motion, a preliminary of damage assessment of the building structure can be examined.

5.3 Analysis of a standard-type 4-story elementary school building

In this study, a standard-type 4-story elementary school building located at Hwa-Lian (Taiwan) is selected. A series of seismic responses recorded from this building between 1994 and 2010. Fig. 17(a) shows the distribution of accelerometers in the building. Fig. 17(b) shows the distribution of the recorded maximum roof peak acceleration (PA) for each seismic event starting from the installation of seismic monitoring system. Among these events five seismic events (i.e., Event-4, -5, -6, -13 and -31) from the acceleration response of roof at sensor #22 along X-direction (longitudinal direction) and at sensor # 19 along Y-direction (transverse direction) were selected to examine the time-frequency representation of the building during earthquake using MCMW-VCF method. This building had been retrofitted twice: one is after the Chi-Chi earthquake and the other is in the year of 2010. Event-4 and Event-6 are two small events before and after the Chi-Chi earthquake (Event-5), and Event-13 (after 1st-stage retrofit of the building) and Event-31 (after 2nd stage retrofit of the building) are two small seismic events. Fig. 18 shows the time-frequency distribution of the data along X- and Y-direction (using σ=2 in the modified complex Mohlet wavelet). From the observation of the ridge of the spectrogram generated from these five earthquake event data, the lowest dominant frequency can be identified from Event-5 (i.e., Chi Chi earthquake)

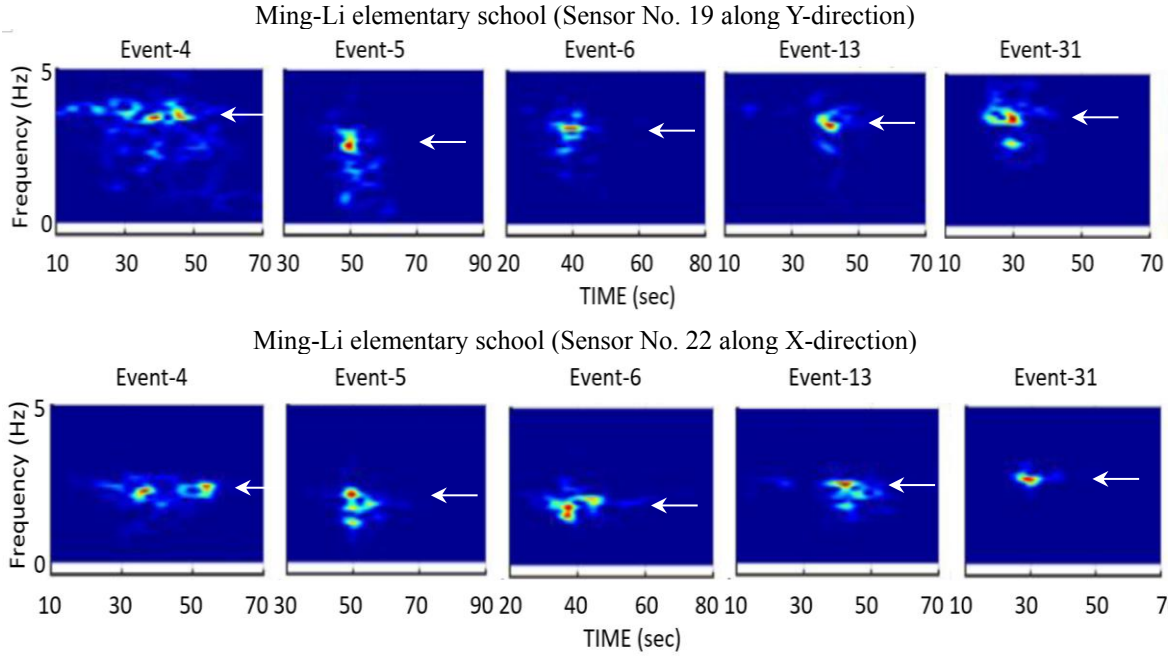

Fig. 18 Time-frequency distribution of five earthquake event data from sensing node 19 (Y-direction) and sensing node 22 (X-direction)

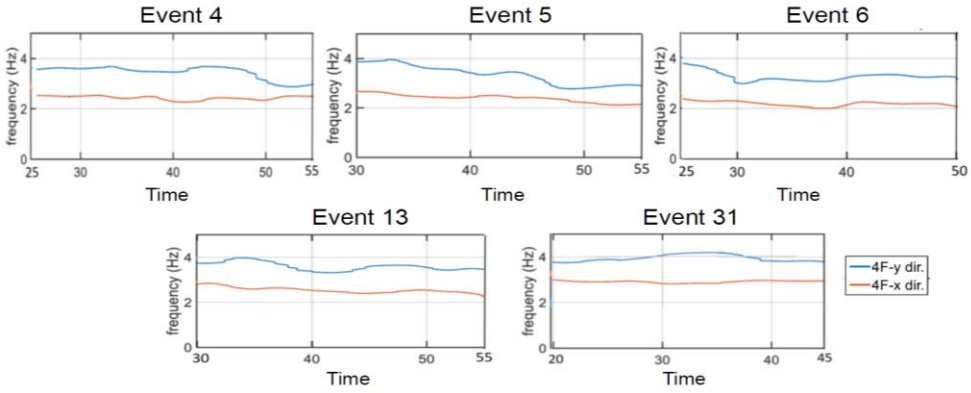

Fig. 19 Identified instantaneous frequency of Ming-Li school building under a series of five Different earthquake excitation

in both X- and Y-directions. Then dominant frequency in Event-14 and Event-31 is much higher than the Event-4 and Event-5, because after the Chi-Chi earthquake the building was retrofitted and strengthened. It is also observed that the identified dominant frequency of the building after retrofit can reach to the original building dominant frequency in both directions. It is summarized that the time-frequency representation of building seismic response data can provide a quick safety assessment of the building through the change of system dominant frequency.

To provide a better visualization on the change of ridge in the spectrogram along time axis, the pseudo IF is calculated from each spectrogram based on Eq. (7). Since the absolute acceleration data

is strongly influenced by the ground level acceleration, therefore, the relative acceleration data is used (between roof response and ground level excitation) is used to estimate pseudo-IF. Fig. 19 shows the identified pseudo-IF from sensing node-19 (Y-direction) and sensing node-22 (X) of the school building under a series of five different earthquake excitation. From the identified pseudo-IF the degradation of frequency is obvious in the event-5 than other event because of the damage during Ch-Chi earthquake. Since the building was retrofitted twice after Chi-Chi earthquake, therefore, the identified pseudo-IF for event 31 increased. It is also recognized that the identified dominant frequency of the school building is higher in Y-direction than in X-direction. Comparison the result with respect to identify the time-vary system frequency using recursive subspace identification (RSI) (Loh *et al*. 2017), the proposed method can provide a fast safety assessment of the structure without any complicated analysis such as RSI.

6. Conclusions

Time-frequency analysis methods allow for the investigation of signals with evolving frequency content. The modified wavelet transformation (including related techniques such as the selection of suitable model parameters) allows for high resolution representation in the time-frequency plane compared with Fourier and tradition wavelet analysis, within the constraints of the uncertainty principle. Through this study the following conclusions are drawn:

1. This increase in resolution makes advanced time-frequency analysis method a useful tool for investigating the dynamic properties of instrumented systems. The original scalogram was replaced by the spectrogram which can provide an easy and clear time-frequency representation of the measured data.
2. In the case of instrumented structures under earthquake excitation, the proposed modified complex Mohlet wavelet with the variable central frequency, the reduced interference distribution can be considered for revealing information about the onset and extent of changes in observed apparent frequency. The changes in frequency content of the signal can then be correlated with physical changes to the system.
3. As compared to the recursive subspace identification on the estimation of time-varying system dominant frequency, the proposed time-frequency method can provide a more direct and effective way of the estimation of system instantaneous frequency. It provides a quick and reliable way for structural damage identification, since the changes in the physical properties of a system (from nonlinearity, loss of stiffness, or damage) are represented in the time-frequency plane as changes in frequency content.

Acknowledgments

This research was supported by the U.S. Department of Conservation for the California Strong Motion Instrumentation Program (CSMIP) data interpretation project no. 1018-567.

References

Ali, S.B. and Kim, D. (2017), “Wavelet analysis of soil-structure interaction effect on seismic response of

base-isolated nuclear power plants", *Earthq. Struct.*, **13**(6), 561-572. https://doi.org/10.12989/eas.2017.13.6.561.

Allen, J.B. and Rabirier, L.R. (1977), "An unified approach to short-time Fourier analysis and synthesis", *Proc. IEEE*, **65**(11), 1558-1564. https://doi.org/10.1109/PROC.1977.10770.

Chen, J.D. and Loh, C.H. (2017), "Tracking modal parameters of building structures from experimental studies and earthquake response measurements", *Struct. Hlth. Monit.*, **16**(5), 551-567. https://doi.org/10.1177/1475921717696339.

Chen, J.D. and Loh, C.H. (2018), "Two-stage damage detection algorithms of structure using modal parameters identified from recursive subspace identification", *Int. J. Earthq. Eng. Struct. Dyn.*, **47**(3), 573-593. https://doi.org/10.1002/eqe.2980.

Golyandina, N., Nekrutkin, V. and Zhigljavsky, A.A. (2001), *Analysis of Time Series Structure: SSA and Related Techniques*, Chapman and Hall/CRC.

Guo, Y. and Kareem, A. (2015), "System identification through nonstationary response: wavelet transformed singular value decomposition-based approach", *J. Eng. Mech.*, **141**(7), 04015013. https://doi.org/10.1061/(ASCE)EM.1943-7889.0000905.

Kijewski, T. and Kareem, A. (2003), "Wavelet transforms for system identification in civil engineering", *Comput. Aid. Civil Infrastr. Eng.*, **18**(5), 339-355. https://doi.org/10.1111/1467-8667.t01-1-00312.

Klepka, A. and Uhl, T. (2014), "Identification of modal parameters of non-stationary systems with the use of wavelet based adaptive filtering", *Mech. Syst. Signal Pr.*, **47**(1-2), 21-34. https://doi.org/10.1016/j.ymssp.2013.09.001.

Lardies, J. and Ta, M.N. (2005), "A wavelet-based approach for the identification of damping in non-linear oscillators", *Int. J. Mech. Sci.*, **47**(8), 1262-1281. https://doi.org/10.1016/j.jimecsci.2005.04.010.

Lee, S.G., Yun, G.J. and Shang, S. (2014), "Reference-free damage detection for truss bridge structures by continuous relative wavelet entropy method", *Struct. Hlth. Monit.*, **13**(3), 307-320. https://doi.org/10.1177/1475921714522845.

Li, H.N., Yi, T.H., Ren, L., Li, D.S. and Huo, L.S. (2014), "Reviews on innovations and applications in structural health monitoring for infrastructures", *Struct. Monit. Mainten.*, **1**(1), 1-45. http://doi.org/10.12989/smm.2014.1.1.001.

Michel, C. and Gueguen, P. (2010), "Time-frequency analysis of small frequency variations in civil engineering structures under weak and strong motions using a reassignment method", *Struct. Hlth. Monit.*, **9**(2), 159-172. https://doi.org/10.1177/1475921709352146.

Nair, K.K. and Kiremidjian, A.S. (2009), "A damage detection algorithm using the morlet wavelet transform", Technical Report, Stanford University.

Noh, H., Nair, K.K. and Kiremidjian, A.S. (2011), "Use of wavelet-based damage-sensitive features for structural damage diagnosis using strong motion data journal of structural engineering", *J. Struct. Eng.*, **137**(10), 1215-1228. https://doi.org/10.1061/(ASCE)ST.1943-541X.0000385.

Taha, M.R., Noureldin, A., Lucero, J.L. and Baca, T.J. (2006), "Wavelet transform for structural health monitoring: a compendium of uses and features", *Struct. Hlth. Monit.*, **5**(3), 267-295. https://doi.org/10.1177/1475921706067741.

Tarinejad, R. and Damadipour, M. (2014), "Modal identification of structures by a novel approach based on FDD-wavelet method", *J. Sound Vib.*, **333**(3), 1024-1045. https://doi.org/10.1016/j.jsv.2013.09.038.

Todorovska, M.I. (2001), "Estimation of instantaneous frequency of signals using the continuous wavelet transform", Report CE 01-07, Dept. of Civil Eng., Univ. of Southern California, CA, USA.

Yen, G.G. and Lin, K.C. (2002), "Wavelet packet feature extraction for vibration monitoring", *IEEE Trans. Indus. Electron.*, **47**(3), 650-667. https://doi.org/10.1109/41.847906.